Powder Technology 367 (2020) 225–232

Contents lists available at ScienceDirect

Powder Technology

journal homepage: www.elsevier.com/locate/powtec

Effect of titanium hydride powder addition on microstructure and properties of titanium powder injection molding

Kai Hu [a,b], Liming Zou [a,*,1], Qi Shi [a], Ke Hu [a], Xin Liu [a,*,1], Bohua Duan [b,*,2]

[a] Guangdong Institute of Materials and processing, Guangdong Academy of Sciences, Guangzhou 510650, China
[b] School of Meterials Science and Engeering, Central South University, Changsha 410083, China

ARTICLE INFO

Article history:
Received 16 July 2019
Received in revised form 6 December 2019
Accepted 24 March 2020
Available online 27 March 2020

Keywords:
Titanium
Metal injection molding
TiC
Composite
Microstructure
Mechanical properties

ABSTRACT

Titanium hydride powder was used to completely or partly replace the spherical titanium powder in order to reduce the cost. The microstructure and mechanical properties after debinding and sintering were investigated. The results showed that with the addition of the titanium hydride powder, the microstructure gradually changed. The fabricated alloy was a titanium matrix composite reinforced with in-situ TiC particles. With the increase in the proportion of titanium hydride powder, the catalytic debinding percentage decreased, which led to an increase in the concentration of carbon and oxygen, and hence, there was a decrease in the tensile strength and elongation though the density of titanium MIM samples increased. The hardness and wear resistance increased as compared with those for pure titanium materials in the market. These results provide a promising method for reducing the cost of titanium MIM, and development of great industrial application prospects.

1. Introduction

As a high-quality, light metal structural and functional material, titanium has low density, high specific strength, good biocompatibility, oxidation resistance, corrosion resistance, non-magnetic properties and non-toxic properties, etc. The metal has always played a major role in the fields of aerospace, medical equipment, chemical production, and military manufacturing [1–3]. However, a high manufacturing cost and poor processing performance greatly limit the large-scale applications of titanium [4–6]. Also, titanium is chemically active and easily reacts strongly with elements such as C, N, O, and H [7–11]; hence, the presence of these elements can seriously affect the performance of titanium products. Therefore, it is necessary to prevent titanium from contamination during processing; thus, increasing the equipment expenditure. Therefore, a reduction in the cost of titanium products and enhancement of the processing technology of titanium has always been the focus and challenge for researchers.

Metal Injection Molding (MIM) is a near-net forming technology that incorporates modern plastic injection molding technology with the field of powder metallurgy [12–14]. The technology has a cost advantage in the preparation of small and complex shape products, and effectively solves the problem of difficult processing of titanium products [15–18]. However, to improve the injection fluidity [19], expensive spherical titanium powder is used as a raw powder in MIM, resulting in an increase in the cost. In order to solve this problem, some researchers have used HDH titanium powder [12,20] and titanium hydride powder [21,22] instead of spherical titanium powder for MIM. Dehghan-Manshadi [20] et al. prepared MIM samples using inexpensive non-spherical HDH titanium powder which achieved a tensile strength of 395 MPa and elongation of 12.5%. Also, German [12] prepared MIM samples using a mixture of HDH titanium powder and gas atomized titanium powder as the raw material, and the solid loading of the feedstock reached 72%. Some researchers have confirmed that titanium hydride powder can also be applied to MIM. Eric Nyberg [21] et al. formed MIM titanium samples by the process using naphthalene as the principal binder constituent and titanium hydride powder as the raw material, and it was found that tensile strengths comparable to wrought titanium could be achieved; however, the maximum elongation was less than expected. Carreño-Morelli [22] et al. used pure titanium hydride powder as the raw material for wax-based binder system, wherein the MIM samples achieved good elongation and tensile strength after solvent debinding, thermal debinding and sintering at 1200 °C for 2 h. However, still, there is limited research on the titanium MIM using titanium hydride powder as raw material for the mainstream POM-based binder systems. In this study, titanium hydride powder and spherical titanium powder were mixed in different weight

* Corresponding authors.
E-mail addresses: lmzou@mail.scut.edu.cn (L. Zou), shaneliu118@163.com (X. Liu), duan-bh@csu.edu.cn (B. Duan).
[1]Postal address: NO.363, Changxin Road, Guangzhou city, Guangdong Province, China.
[2]Postal address: No.932, South Lushan Road, Changsha city, Hunan Province, China.

https://doi.org/10.1016/j.powtec.2020.03.059
0032-5910/

Table 1
Powder characterization.

Powder	Powder particle size/(μm)		C content/%	O content/%	Cost/($/kg)
	D50	D90			
TiH_2	14.9	30	0.018	0.3	30
Spherical Ti	16.6	28.0	0.011	0.1	280

proportions as raw materials and POM-based binder system was used. The microstructure and properties of the MIM samples with different ratios of two raw material powders were investigated.

2. Experimental

Angular titanium hydride powder (Tech-long Metal Materials Inc., China) and the spherical titanium powder prepared via inert gas atomization (TSL Materials Inc., Germany) were used in this study. The characteristics of two powders are listed in Table 1, while the powder morphology is shown in Fig. 1. Four powder ratios were selected for the comparative tests. The raw materials for sample T1 and sample T4 were pure titanium hydride powder and pure spherical titanium powder, respectively. The raw materials for sample T2 and sample T3 were a mixture of titanium hydride powder and spherical titanium powder in the mass ratio of 3:2 and 2:3, respectively.

Feedstocks for powder injection molding were prepared with a POM-based binder system consisting of 88 wt% polyoxymethylene (POM), 5 wt% ethylene-vinyl acetate (EVA), 5 wt% high-density polypropylene (HDPE), and 2 wt% stearic acid (SA). The solids loading, referring to volume ratios of powder in feedstock, were T1 = 50 vol%, T2 = 52 vol%, T3 = 56 vol%, and T4 = 60 vol%, respectively. The mixing was performed in a mixer (CF-1LKH, CFen corp, China) in an Ar atmosphere at 180 °C for 90 min. The cooled feedstock was broken down into millimeters of injected feedstock using a crusher. The tensile test samples conforming to the ASTM standards were injection molded in an injection molding machine (320C, Arburg GmbH, Germany) at maximum injection pressure of 95 MPa. The injection temperature from the barrel to nozzle were 155 °C, 175 °C, 180 °C, 185 °C, and 195 °C. Catalytic debinding was performed in a catalytic debinding furnace (HT-220LTZL, Winteam Corp, China) at 120 °C for 8 h with nitric acid as the catalytic medium. This process was primarily used to remove POM. Thermal debinding, dehydrogenation, and sintering process were performed at 10^{-3} Pa vacuum in a vacuum sintering furnace (ZHJ-90-16 W, Lanzhou Vacuum Corp, China).

The density of sintered samples was measured via Archimedes method, five samples were measured and then averaged, and then, the ratio of actual density to theoretical density was calculated to obtain the relative density of the sintered samples. The metallographic preparation of sintered samples was performed via grinding and polishing. Afterwards, the grain boundary was etched using a mixture of hydrofluoric acid, nitric acid and distilled water in the volume ratio of 1:5:14. The morphology of powders and microstructure of debinding and sintered samples were observed under a scanning electron microscope (JXA-8100, JEOL, Japan). The Vickers hardness of sintered samples was measured via the Vickers microhardness tester (ZHU-S, Indentec, UK). At the surface of the sample, hardness was measured on 7 points in the direction from the edge to the center with the constant spacing. Then, the maximum and minimum values were removed and the average of the remaining five numbers was taken as the final hardness of the tested sample. The dry sliding wear properties of the sintered samples against 45 carbon steel were evaluated using a wear and abrasion test machine (MMG-5, Hanseng Corp, China), wherein, the pressure was 50 N, the rotation speed was set to 50 r/min, and the wear time was set to 10 min. The tensile properties of the sintered samples were measured using electronic stretching machine (Instron8801, Instron, USA). The phase analysis of sintered samples was performed by X-ray diffraction (XRD) (D/MAX-2500/PC, Raigaku Corp, Japan). The phase structure and interface characteristics of sintered samples were observed under transmission electron microscope (JEM-2100F, JEOL, Japan). DSC-TG tests of feedstock were performed via synchronous differential thermal analyzer (STA 409 PC/PG, NETZSCH, Germany). The contents of interstitial elements O, H, and C in powders and sintered samples were determined using oxygen/nitrogen/hydrogen determinator (ONH836, LECO, USA) and carbon/sulfur determinator (CS600, LECO, USA), respectively.

3. Results and discussion

3.1. DSC-TG

Fig. 2a, b display the DSC-TG curves for the feedstock prepared from titanium hydride powder and spherical titanium powder, respectively. As shown in Fig. 2a, there were three clear endothermic processes. The first stage interval was 158.7 °C–171.5 °C with the peak at 166.5 °C. The second stage interval was 282 °C–381.6 °C with the peak at 294.3 °C. The third stage interval was 424.9 °C–607 °C with the peak at 497.3 °C. There were two distinct stages of mass changes in the TG curve. The first stage ranged from 243.3 °C–405.9 °C, wherein the quality of feedstock was reduced by 8.92%. The second stage ranged from 405.9 °C–509.3 °C, wherein the quality of feedstock was reduced by 2.25%. As shown in DSC curves in Fig. 2b, there were two clear endothermic processes. The second interval was 163.6 °C–170.5 °C with the peak at 168.4 °C. The second interval was 280.7 °C–410.5 °C with the peak at 330.7 °C. There were two distinct stages of mass change in the TG curve.

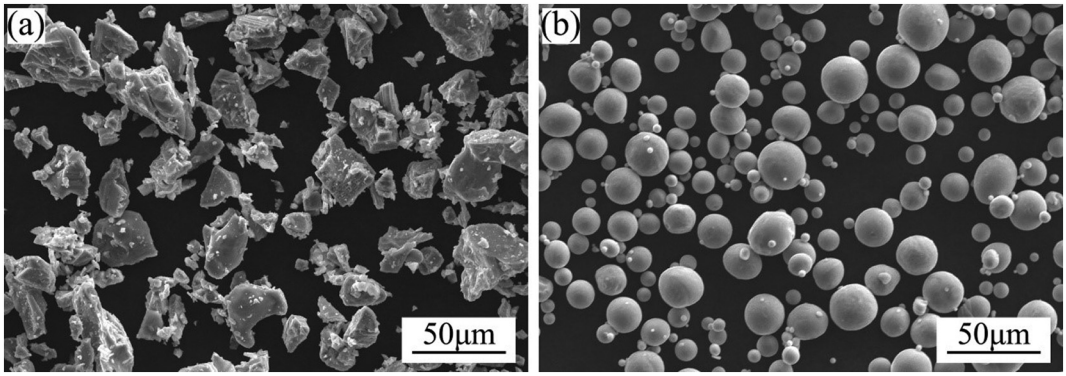

Fig. 1. SEM image of powders: (a) Titanium hydride powder, (b) Spherical Titanium powder.

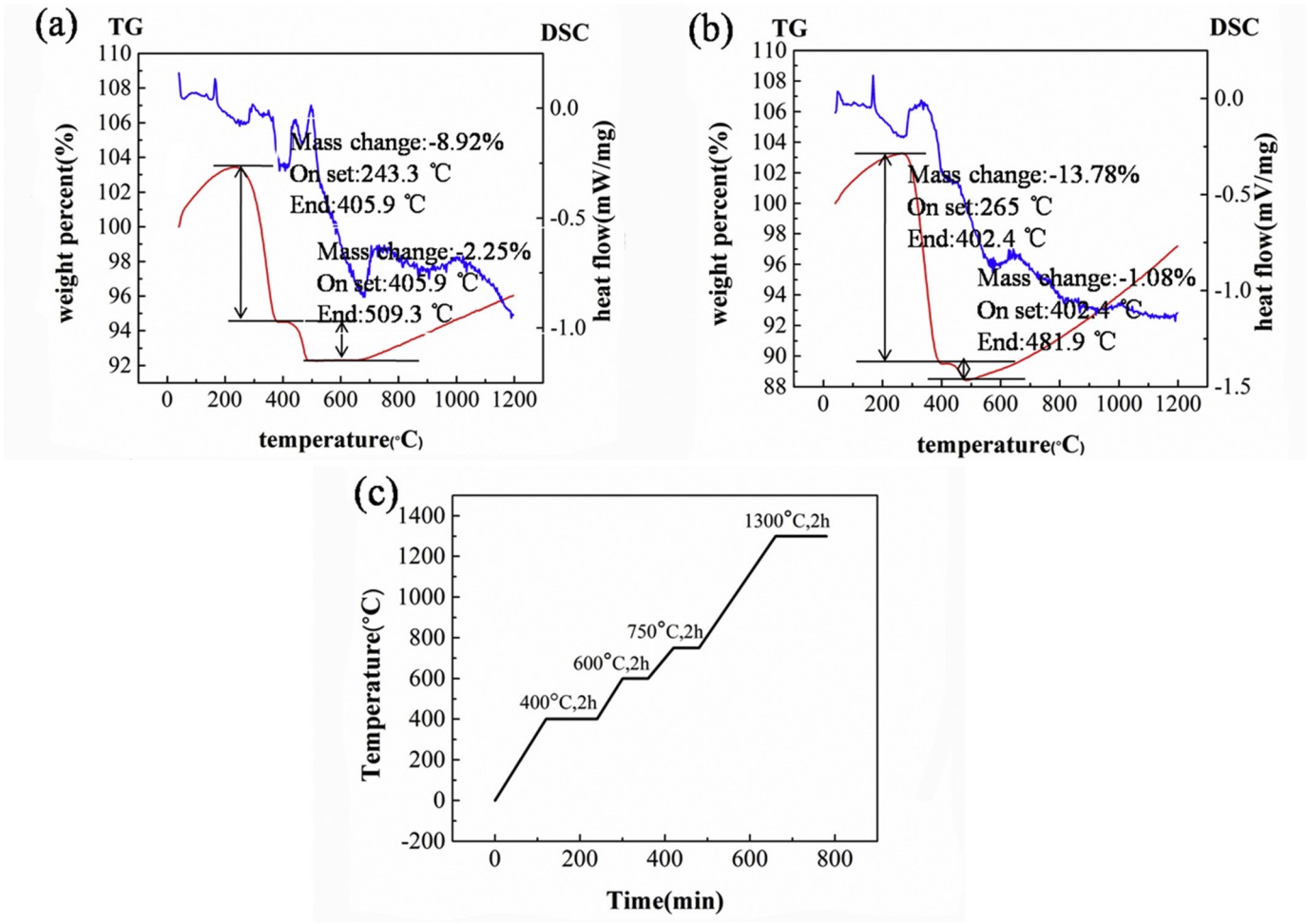

Fig. 2. DSC-TG curve of feedstock: (a) T1, (b) T4. (c) process of sintering for sample T1,T2, and T3.

The first stage ranged from 265 °C–402.4 °C, wherein the quality of feedstock was reduced by 13.78%. The second stage ranged from 402.4 °C–481.9 °C, wherein the quality of feedstock was reduced by 1.08%. Interestingly, the mass loss in sample T1 was lower than that in sample T4, inspite of the solid loading of sample T1(50 vol%) being lower than the sample T4 (60 vol%), and hence there is more binder in sample T1, the mass loss in sample T1 should have been higher than that in sample T4. The reason for the phenomenon is that the binder in sample T1 was not easily removed due to the irregular morphology of titanium hydride powder, some debinding path might have been blocked, while the morphology of spherical titanium powder is regular and the binder in sample T4 could be easily removed. Therefore, the mass loss in sample T1 was lower than that in sample T4. These results are consistent with the results of the debinding percentage of samples presented later in the paper.

The DSC curves in Fig. 2a, b were approximately the same in the first two endothermic phases. The main reason for the heat absorption is the decomposition and volatilization of the binder. The dehydrogenation transition of titanium hydride is $TiH_2 \rightarrow TiHx \rightarrow \alpha\text{-}Ti$ $(0.7 < x < 1.1)$ [23-25], which occurs between the temperature range of 400 °C–800 °C and 500 °C–550 °C is the main dehydrogenation stage [26]. Therefore, the third significant endothermic reaction in Fig. 2a at the temperature range of 424.9 °C–607 °C can be explained by the dehydrogenation reaction of titanium hydride powder during heating.

As same binder system was used, the weight loss stages shown in Fig. 2a and b were approximately the same. In combination with the decomposition temperature of each component of the binder, we infer that POM and SA decomposed and volatilized at 265 °C–410 °C, while EVA and HDPE decomposed and volatilized at 405 °C–510 °C [27]. The determination of the sintering process for sample T1, T2, and T3 was based on the results of the DSC-TG experiments (Fig. 2c). The aim of holding for 2 h at 750 °C was a thorough promotion of dehydrogenation. The final sintering temperature was set as 1300 °C and held for 2 h.

3.2. Catalytic debinding percentage and density

Fig. 3a, c shows the SEM images of feedstock T2 and T4, and it can be seen that the feedstock T4 was more uniformly mixed than the feedstock T2, and the binder was uniformly wrapped around the surface of spherical titanium powders. The reason can be explained by the fact of good fluidity and low friction between the spherical powders. Due to the presence of irregular titanium hydride powder in the feedstock T2, there was high friction between the powders; hence, the mixing between the powder and the binder was not uniform. Fig. 3b, d show the SEM images of samples T2 and T4 after catalytic debinding which was primarily used to remove POM [26]. It was observed that more binder remained around the powder of sample T2, most of which adhered to the irregular titanium hydride powder surface. This

phenomenon can be related to the irregular morphology of the titanium hydride powder. The interconnected paths were formed between the spherical powders, which could aid in discharging the binder steam under high temperature. However, when spherical titanium powders were mixed with titanium hydride powders, some paths might have been blocked, and hence, the discharge of the binder steam was reduced due to rough surface and polygonal shape of titanium hydride powders. As shown in Fig. 3e, the catalytic debinding percentage, which means ratio of removed POM to total, for sample T1, T2, T3 and T4 were 47.48%, 68.87%, 81.54% and 99.55%, respectively.

These results indicate that POM within the feedstock prepared using spherical titanium powder could basically be removed after catalytic debinding. More addition of titanium hydride powder led to more residual POM amount. In addition, as shown in Fig. 3e, the relative density of the sintered samples T1, T2, T3, and T4 reached 99.48%, 98.02%, 97.8%, and 96.76%, respectively. These results suggest that the sintered density of the samples became higher with the addition of titanium hydride powder. The reason is the phase change mechanism of titanium hydride powder during the dehydrogenation process and the effect of atom-attenuating the Ti—Ti bond energy, which could increase the diffusion coefficient of the atoms; thereby, accelerating the sintering process and making the product denser [28,29].

3.3. Microstructure characterization

Fig. 4 shows the microstructure of four kinds of sintered samples. The microstructure of sintered sample T1 (Fig. 4a) was the typical equiaxed structure [30], composed of equiaxed α-Ti phase (area A, large globular grains) and a small amount of intergranular β-Ti (area B, island-like grains), which was distributed between the α-Ti phase. Some fine dot-shaped precipitates with the size of 5–10 μm (area C) existed within the α-Ti phase. The precipitates proved to be TiC in the later energy spectrum analysis. Few pores existed in the sintered sample T1, which is consistent with its high relative density. The microstructure of the sintered sample T4 (Fig. 4d) was the typical basketweave [30]. In the process of α → β phase transition, the β phase needs to be heated or held for some time to reach a steady state. In this study, the β grains were heated in the full β phase (1300 °C) for a sufficient period of time (2 h); at this moment, β phase was in equilibrium state. During the cooling process, due to the low nucleation driving force in the high temperature stage, α grains preferentially nucleated at the β grain boundary, forming grain boundary α phase. Afterwards, the grain boundary α induced nucleation at the α/β boundaries to form α colonies, which grow into the β grains until they encounter other oriented α colonies that grow out of the other β boundaries and eventually

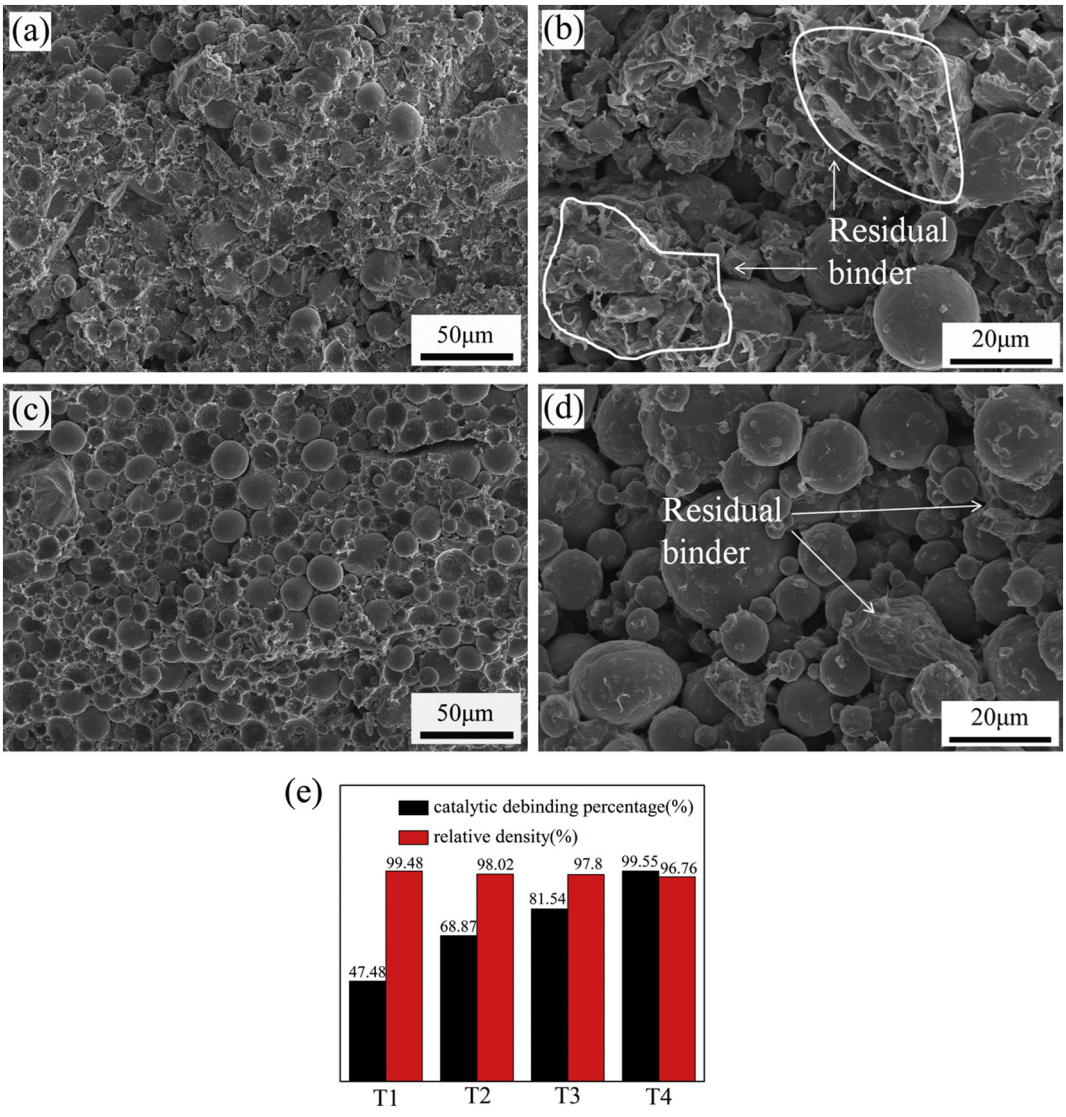

Fig. 3. SEM image of feedstock: (a) T2, (c) T4. SEM image of sample after catalytic debinding: (b) T2, (d) T4. (e) catalytic debinding percentage and relative density of samples.

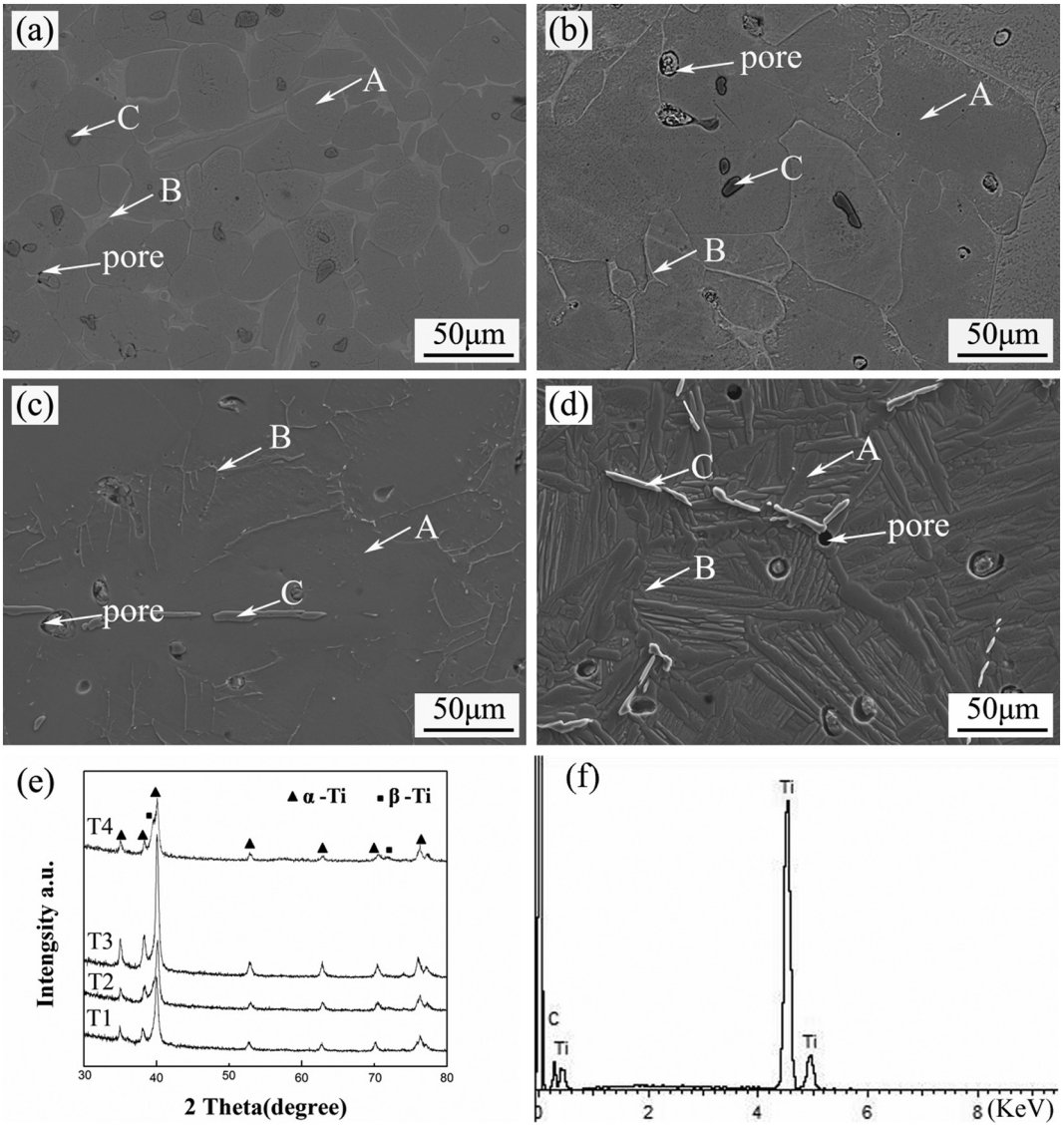

Fig. 4. SEM image of sintered sample: (a) T1, (b) T2, (c) T3 and (d) T4. (e) XRD patterns of sintered samples. (f) EDS data of area C in sample T1.

form α structure. In addition, because the furnace cooling method was adopted in this study, the cooling rate was slow, which provided more time for the growth of grain boundary and the α layer was thicker (10 μm) [5]. The original β grain boundaries were destroyed. The morphology of α-Ti phase was lamellar. The precipitates were also observed in the sintered sample T4, whose morphology was stripy and the size was from 5 to 20 μm. A few circular pores existed in the sintered sample T4, as indicated in Fig. 4b. The microstructures of the sintered samples T2 (Fig. 4b) and T3 (Fig. 4c) were composed of the bimodal structure (equiaxed α-Ti phase and coarse lamellar α-Ti phase) and small amount of intergranular β-Ti phase, the precipitate was an irregular sheet-like structure with a size of 10–50 μm. Some circular pores also existed in the microstructure. With the increase in titanium hydride powder content, the morphology of precipitate changed from stripy to dot-shaped. The phase size of sintered sample T3 was finer than that for the sample T2. For four kinds of sintered samples, composite with in-situ TiC phase was eventually obtained. The difference in microstructure for the sintered samples can be attributed to difference in raw materials. The phase of the spherical titanium powder was dendrite because of the rapid cooling during gas atomization [31]. The microstructure of the sample after pressing and sintering was primarily basketweave [31]. The dehydrogenation transition happened for titanium hydride powder during the sintering process; hence, the primary equiaxed α-Ti phase was generated. For the wax-based and water-soluble based system binder, no precipitation of TiC has been reported [[22,32]]. This may be related to different binder composition.

The different areas were analyzed via EDS to identify the phase compositions. For areas A and B, the composition was mainly Ti. Fig. 4f shows the EDS data of area C in sample T1, and the elemental composition of area C is presented in Table 2. For the four samples, the composition of area C was Ti and C element, which suggests that the precipitate was TiC phase. The TiC hard phase was formed by the in-situ complex reaction of the Ti element and C element from the binder at high temperatures during the sintering process [33] [34]. As α stabilizer [5], carbon is easy to aggregate in the α-Ti phase. During the heating process, the C element from residual binder reacts with α-Ti phase to form TiC, and the growth of TiC is related to the formation of the α-Ti phase. Therefore, the difference in morphology of TiC phase is related to the morphology of the α-Ti phase in the sintered samples. The morphology of α-Ti phase in the sintered sample T1 was equiaxed, while the morphology of the TiC phase was dot-shaped. The morphology of the α-Ti phase in the sintered samples T2 and T3 was

Table 2
The chemical composition of area C in sintered samples.

Sample	C content/%	Ti content/%
T1	15.34	84.66
T2	13.54	86.46
T3	12.70	87.30
T4	13.71	86.29

Table 3
Mechanical properties and impurity content of the sintered samples.

Sample	T1	T2	T3	T4	Ti grade 4[a]
σ/MPa	319	507	683	838	550
$\sigma_{0.2}$/MPa	163	405	543	729	483
δ/%	1.1	2.7	5.1	6.3	15
Hardness/HV	454	389	353	330	221
Abrasion loss/mg	6.7	8.4	7.9	10.5	14.6
C content/%	0.22	0.18	0.16	0.12	0.08
O content/%	0.67	0.48	0.37	0.30	0.4
H content/%	0.005	0.003	0.002	0.003	0.015

[a] ASTM Ti grade 4 specification.

irregular and the morphology of TiC phase was also irregular. However, the TiC hard phase in the sintered sample T3 had a tendency to become stripy. The morphology of α-Ti phase in the sintered sample T4 was lamellar, and the morphology of TiC phase was stripy. In addition, we semi-quantitatively calculated the percentage of TiC in each sample via Imagine pro software. The results show that the percentage of TiC in sample T1, T2, T3, and T4 was 2.64%, 2.32%, 2.16% and 1.81%, respectively. The content of TiC should have a relationship with the solid loading. Smaller the solid loading, higher is the content of binder in the feedstock. The content of TiC which was formed by the in-situ complex reaction of the Ti element and C element from the binder improved with increasing solid loading. The area A and B of the four samples were α-Ti phase and β-Ti phase, respectively. The XRD curves of the sintered samples are shown in Fig. 4e. The phase of the four sintered samples was primarily composed of α-Ti phase and a small amount of β-Ti phase. The TiC phase could not be detected as probably it was extremely less. These results are consistent with the microstructure of the sintered samples.

Fig. 5a shows a typical low-magnification transmission electron microscopy (TEM) image of the sintered sample T4 after tensile test. The corresponding selected area electron diffraction (SAED) patterns (Fig. 5c, d) can be analyzed that the gray region was the β-Ti phase while the black region was the α-Ti phase. TiC particles existed in the α-Ti matrix. As shown in Fig. 5a, there were numerous dislocation lines in the α-Ti phase. As shown in the zoom in version of the junction area between the two phases (Fig. 5b), the dislocation line was stacked at the intersection of the α-Ti phase and β-Ti phase by the slip motion to form a stacking fault. The stacking fault appeared as a clear step structure from Fig. 5b.

3.4. Mechanical properties

The mechanical properties of the sintered samples are presented in Table 3. With the decrease in the titanium hydride powder, the tensile strength and plasticity of the samples increased gradually. When pure spherical titanium powder was used as the raw material (Sample T4), the tensile strength reached 838 MPa while the elongation reached 6.3%, the tensile strength of the sintered sample T4 far exceeded that of ASTM titanium grade 4 (550 MPa). The reason for the phenomenon is that, on one hand, a large number of lamellar α staggered arrangement increased the phase interface and deformation resistance; thereby, increasing the strength of the sample T4 [35]. On the other hand, the in-situ TiC phase formed a titanium matrix composite, which greatly enhanced its tensile strength but also reduced its elongation. For the sintered sample T1, although its relative density was the highest, but its tensile properties were the worst among all the samples. Although the presence of equiaxed α could improve the plasticity of the

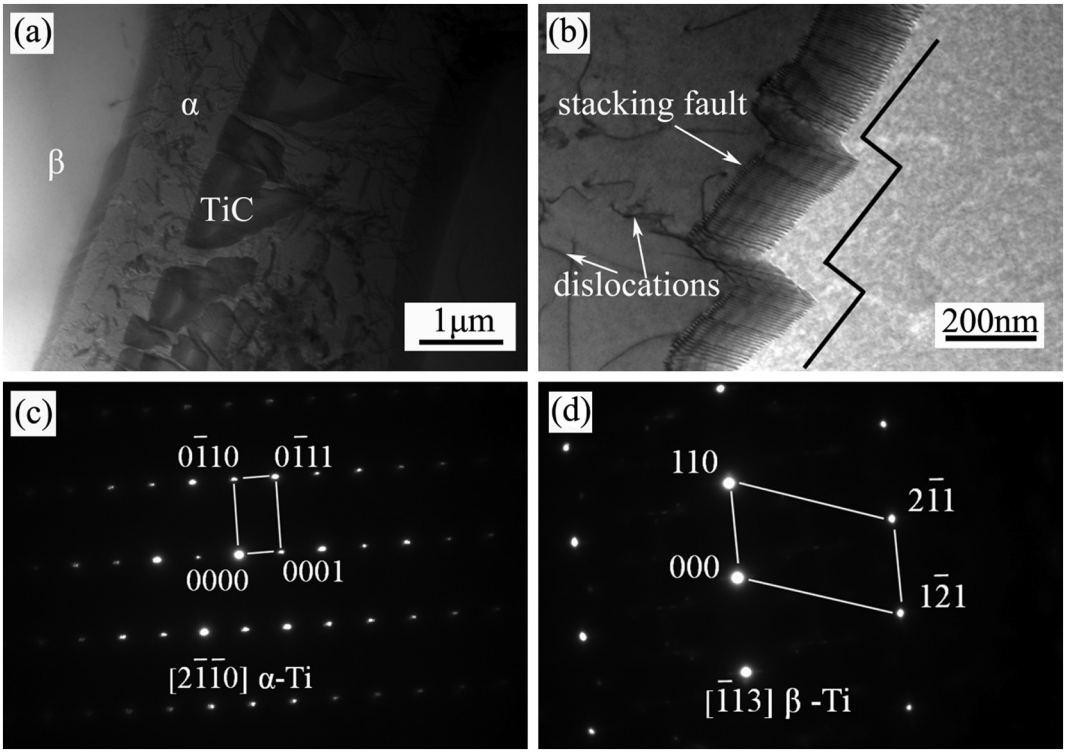

Fig. 5. (a) TEM image of the sintered sample T4, (b) dislocation accumulate at the α/β phase boundary, (c) and (d) corresponding SAED patterns of α-Ti phase and β-Ti phase.

titanium products [5], excessive carbon and oxygen content could still seriously damage its plasticity [35]. It is reported that the release of hydrogen from titanium hydride powder can inhibit the oxidation of titanium during the sintering process [36,37]. However, during the catalytic debinding process in this study, irregular titanium hydride powder blocked the path and POM could not be removed completely (as discussed earlier in the paper). During subsequent thermal debinding and vacuum sintering, residual binder decomposition led to titanium contamination, resulting in a significant increase in the oxygen and carbon content. In addition, as shown in Fig. 1, the surface of titanium hydride powder was rougher than the spherical titanium powder, and there existed cracks in the titanium hydride powder. It means binder adhered to such cracks is hard to be removed during the debinding and sintering process.

As shown in Table 3, as the titanium hydride powder increased, the catalytic debinding percentage decreased while the oxygen and carbon content increased. For the sintered samples T3 and T4, the oxygen content met the standards for ASTM titanium grade 4, but the carbon content was slightly higher. The higher carbon content led to an increase in the strength of the sample, but also reduced its elongation [38]. The hydrogen content of the samples was far below the standards of ASTM titanium grade 4. These results suggest that the dehydrogenation of titanium hydride powder was thorough during the sintering process. A higher impurity content also led to an increase in the hardness of the sample as compared with the ASTM titanium grade 4, while the wear resistance was also accordingly increased. The abrasion loss for the sintered sample T1 was less than half of that for ASTM titanium grade 4.

In case of the applications such as wearable devices, the requirement of ductility is not strict while the wear resistance is required. Hence, the raw materials mixed with titanium hydride powder and spherical titanium powder can be used to reduce the cost. In addition, the higher relative density contributes to the subsequent polishing processes. The material has potential for such applications because of its excellent wear resistance performance and high relative density.

The fractured surface and worn surface of the sintered samples T2 and T4 are shown in Fig. 6. The fractography of the sintered sample T2 (Fig. 6a) exhibited an apparently brittle mode and only a small number of dimples could be found. It is a typical cleavage fracture. The fractography morphology of the sample T1 was similar to that for sample T2. While the fractography of the sintered sample T4 showed apparent dimple characteristics, which means it had better plasticity, and the fractography morphology of the sample T3 was similar to that for sample T4.

Fig. 6c, d show the morphology of the worn surface of sintered samples T2 and T4. After the wear tests, the sample T4 showed slight plastic deformation under combined action with long-term friction and generated pressure, while the other three samples did not demonstrate the same. For the samples T4, there were noticeable plastic deformation and furrows along the direction of sliding. The primary wear mechanism of samples T2 and T4 was abrasive wear. The flaky wear debris also existed on the worn surface of sample T2. The wear mechanism was the combination of abrasive wear and adhesive wear and the furrows were shallower than those for T4. The worn surfaces of samples T1 and T3 were similar to that of sample T2.

4. Conclusion

The effect of the titanium hydride powder addition on the microstructure and properties of titanium MIM was investigated. With the addition of the titanium hydride powder, the microstructure gradually changed from basketweave to the β-Ti phase distributed with equiaxed α-Ti phase, and in-situ TiC particles were formed with different morphology. The prepared alloy was a TiC particle reinforced titanium matrix composite. Owing to the presence of TiC, the strength, hardness, and wear resistance of the samples were greatly improved as compared to the commercial pure titanium. With the increase in the proportion of titanium hydride powder, the density of the titanium MIM samples was also increased and the catalytic debinding percentage was accordingly decreased. This phenomenon led to an increase in carbon and oxygen

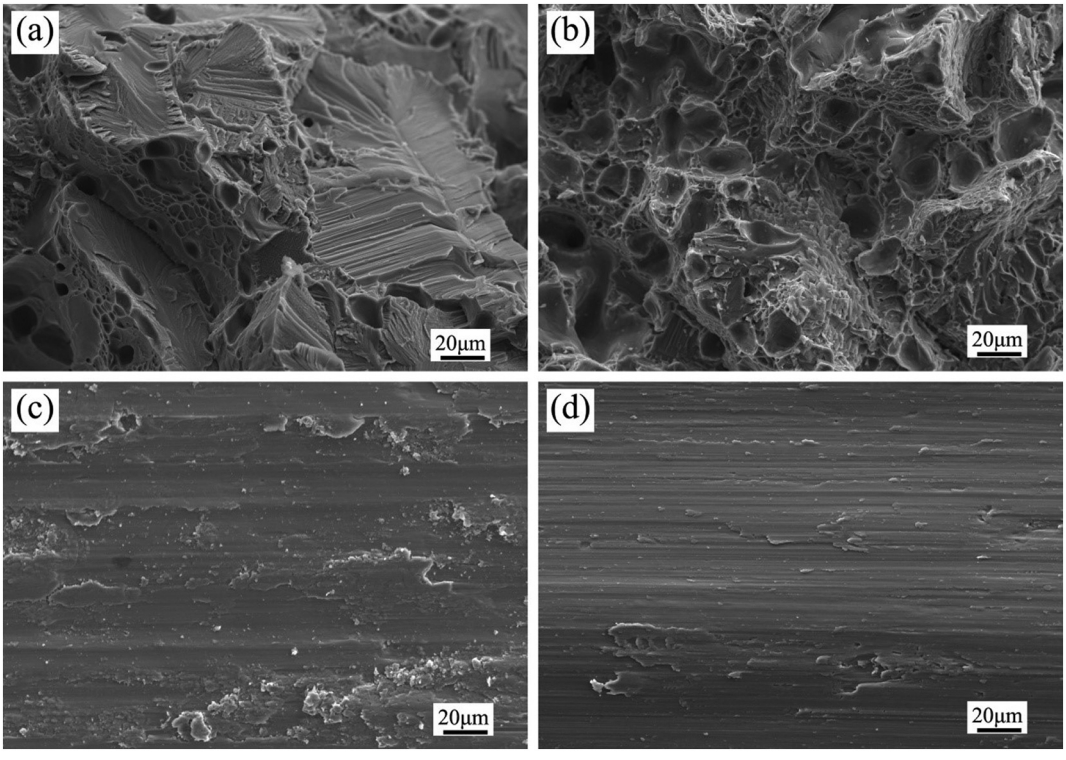

Fig. 6. SEM micrograph of fractured surface of sintered samples: (a) T2, (b) T4. Wear surface of sintered sample: (c) T2, (d) T4.

concentration, and hence, the tensile strength and elongation were decreased. The mechanical properties of the sintered sample T3 (titanium hydride powder and spherical titanium powder with the mass ratio of 2:3) were slightly lower to those for the sintered sample T4 (spherical titanium powder), and the wear resistance was even higher than that of the sintered sample T4. These results suggest that the cost of titanium MIM can be reduced by adding titanium hydride powder, and the material has potential for applications in several fields such as wearable devices.

Acknowledgements

This work was supported by the International Cooperation Program of Guangzhou City (No. 201907010030), the International Cooperation Program of Guangdong Province (No. 2018A050506010), Research and Development Program in Key Areas of Guangdong Province (No.2018B090904004), and the GDAS' Project of Science and Technology Development (No. 2019GDASYL-0402006).

References

[1] F.H.S. Froes, Advances in titanium metal injection molding, Powder Metall. Met. Ceram. 46 (5–6) (2007) 303–310.
[2] C. Cui, B.M. Hu, L. Zhao, S. Liu, Titanium alloy production technology, market prospects and industry development, Mater. Des. 32 (3) (2011) 1684–1691.
[3] D. Banerjee, J.C. Williams, Perspectives on titanium science and technology, Acta Mater. 61 (2013) 844–879.
[4] J.E. Barnes, W. Peter, C.A. Blue, Evaluation of low cost titanium alloy products, Mater. Sci. Forum 618-619 (2009) 165–168.
[5] C. Leyens, M. Peters, Titanium and Titanium Alloys: Fundamentals and Applications, WileyVCH, Köln, 2003.
[6] W. Xu, M. Brandt, S. Sun, J. Elambasseril, M. Qian, Additive manufacturing of strong and ductile Ti-6Al-4V by selective laser melting via in situ martensite decomposition, Acta Mater. 85 (2015) 74–84.
[7] T. Ebel, O. Milagres Ferri, W. Limberg, M. Oehring, F. Pyczak, F.P. Schimansky, Metal injection moulding of titanium and titanium-aluminides, Key Eng. Mater. 520 (2012) 153–160.
[8] F.H. Froes, Getting better: big boost for titanium MIM prospects, Met. Powder Rep. 61 (2006) 20–23.
[9] S. Banerjee, C.J. Joens, Sintering powder metal injection molded (MIM) titanium alloys: in vacuum or argon? Key Eng. Mater. 704 (2016) 5.
[10] W.L. Finlay, J.A. Snyder, Effects of three interstitial solutes (nitrogen, oxygen, and carbon) on the mechanical properties of high-purity, alpha titanium, JOM 2 (2) (1950) 277–286.
[11] R.I. Jaffee, H.R. Ogden, D.J. Maykuth, Alloys of titanium with carbon, oxygen and nitrogen, JOM 2 (1950) 1261–1266.
[12] Randall German, Progress in titanium metal powder injection molding, Materials 6 (8) (2013) 3641–3662.
[13] M. Qian, Metal injection moulding (MIM) of titanium and titanium hydride reviewed at PM titanium, PIM Int. 8 (2013) 67–74.
[14] P.G. Esteban, L. Bolzoni, E.M. Ruiznavas, E. Gordo, PM processing and characterization of ti-7Fe low cost titanium alloys, Powder Metall. 54 (3) (2011) 242–252.
[15] M.D. Hayat, G. Wen, M.F. Zulkifli, P. Cao, Effect of PEG molecular weight on rheological properties of Ti-MIM feedstocks and water debinding behaviour, Powder Technol. 270 (2015) 296–301.
[16] M.D. Hayat, A. Goswami, S. Matthews, T. Li, X. Yuan, P. Cao, Modification of PEG/PMMA binder by PVP for titanium metal injection moulding, Powder Technol. 315 (2017) 243–249.
[17] D. Lin, D. Sanétrník, H. Cho, S.T. Chung, Y.S. Kwon, K.H. Kate, B. Hausnerova, S.V. Atre, S. Park, Rheological and thermal debinding properties of blended elemental Ti-6Al-4V powder injection molding feedstock, Powder Technol. 311 (2017) 357–363.
[18] R.M. German, K.H. Hens, Identification of the effects of key powder characteristics on powder injection molding, Met. Powder Rep. 47 (1992) 55.
[19] C.M. Schwanke, J.C. Menegotto, R.M. Gomes, L. Schaeffer, Commercial pure titanium powders obtained by hydrogen embrittlement, Key Eng. Mater. 189-191 (2001) 264–270.
[20] A. Dehghan-manshadi, D. Stjohn, M. Dargusch, Y. Chen, J.F. Sun, M. Qian, Metal injection moulding of non-spherical titanium powders: processing, microstructure and mechanical properties, J. Manuf. Process. 31 (2018) 416–423.
[21] E. Nyberg, M. Miller, K. Simmons, K.S. Weil, Microstructure and mechanical properties of titanium components fabricated by a new powder injection molding technique, Mater. Sci. Eng. C 25 (2005) 336–342.
[22] E. Carreño-Morelli, J.E. Bidaux, M. Rodríguez-Arbaizar, H. Girard, H. Hamdan, Production of titanium grade 4 components by powder injection moulding of titanium hydride, Powder Metall. 57 (2) (2014) 89–92.
[23] V. Bhosle, E.G. Baburaj, M. Miranova, K. Salama, Dehydrogenation of TiH_2, Mater. Sci. Eng. A 356 (1–2) (2003) 190–199.
[24] G. Chen, P. Cao, NiTi powder sintering from TiH2 powder: an in situ investigation, Metall. Mater. Trans. A 44 (13) (2013) 5630–5633.
[25] G. Chen, K.D. Liss, G. Auchterlonie, H. Tang, P. Cao, Dehydrogenation and sintering of TiH2: an in situ study, Metall. Mater. Trans. A 48 (6) (2017) 2949–2959.
[26] S. Krug, J.R.G. Evans, J.H.H. Ter Maat, Residual stresses and cracking in large ceramic injection mouldings subjected to different solidification schedules, J. Eur. Ceram. Soc. 20 (14–15) (2000) 2535–2541.
[27] S.C. Moldoveanu, Analytical Pyrolysis of Synthetic Organic Polymers, Elsevier, 2005.
[28] X.L. Han, Q. Wang, D.L. Sun, H.X. Zhang, First-principles study of the effect of hydrogen on the ti self-diffusion characteristics in the alpha ti-H system, Scripta Mater. 56 (1) (2007) 77–80.
[29] O.N. Senkov, J.J. Jonas, Effect of phase composition and hydrogen level on the deformation behavior of titanium-hydrogen alloys, Metall. Mater. Trans. A 27 (7) (1996) 1869–1876.
[30] Y.Q. Zhao, Metallographic Map of Titanium and Titanium Alloys, Central South University Press, Changsha, 2011.
[31] Q.B. Kuang, L.M. Zou, Y.X. Cai, X. Liu, H.W. Xie, Microstructure and properties of high temperature titanium alloys with a high Si Content Prepared by powder metallurgy, Mater. Trans. 58 (12) (2017) 1735–1741.
[32] A.T. Sidambe, I.A. Figueroa, H.G.C. Hamilton, I. Todd, Metal injection moulding of CP-Ti components for biomedical applications, J. Mater. Process. Technol. 212 (7) (2012) 1591–1597.
[33] L.J. Huang, L. Geng, H.Y. Xu, H.X. Peng, In situ TiC particles reinforced Ti6Al4V matrix composite with a network reinforcement architecture, Mater. Sci. Eng. A 528 (6) (2011) 2859–2862.
[34] J.Q. Qi, Y.W. Sui, Y. Chang, Y.Z. He, F.X. Wei, Q.K. Meng, Z.J. Wei, Superior ductility in as-cast TiC/near-α Ti composite obtained by three-step heat treatment, Vacuum. 126 (2016) 1–4.
[35] A. Dehghan-Manshadi, M. Bermingham, M.S. Dargusch, D.H. Stjohn, M. Qian, Metal injection moulding of titanium and titanium alloys: challenges and recent development, Powder Technol. 319 (2017) 289–301.
[36] E. Carreño-Morelli, M. Rodriguez-Arbaizar, A. Amherd, J.E. Bidaux, Porous titanium processed by powder injection moulding of titanium hydride and space holders, Powder Metall. 57 (2) (2014) 93–96.
[37] H.T. Wang, Z.Z. Fang, P. Sun, A critical review of mechanical properties of powder metallurgy titanium, Int. J. Powder Metall. 46 (5) (2010) 45–57.
[38] S.B. Guo, X.H. Qu, X.B. He, Influence of sintering temperature on mechanical properties of ti-6Al-4V compacts by metal injection molding, Mater. Sci. Forum 475 (2005) 2639–2642.